 doi:10.20944/preprints202210.0474.v1

Article

Uncertainty Assessment of Flood Hazard due to Levee Breaching

Cédric Goeury*, Vito Bacchi, Fabrice Zaoui, Sophie Bacchi, Sara Pavan and Kamal El kadi Abderrezzak

Électricité de France (EDF), Research and Development Division, National Laboratory for Hydraulics and Environment (LNHE), Chatou, France
* Correspondence: cedric.goeury@edf.fr

Abstract: Water resource management and flood forecasting are crucial societal and financial stakes requiring reliable predictions of flow parameters (depth, velocity), the accuracy of which is often limited by uncertainties in hydrodynamic numerical models. In this study, we assess the effect of two uncertainty sources, namely breach characteristics induced by overtopping and the roughness coefficient, on water elevations and inundation extent. A two-dimensional (2D) hydraulic solver was applied in a Monte Carlo integration framework to a reach of the Loire river (France) including about 300 physical parameters. Inundation hazard maps for different flood scenarios allowed highlighting the impact of the breach development chronology. A special attention was paid to proposing a relevant sensitivity analysis to exam the factors influencing the depth and extent of flooding. The spatial analysis of vulnerability area induced by a levee breach width exhibits that, with increasing the flood discharge, the rise of the parameter influence is accompanied by a more localized spatial effect. This argues for a local analysis to allow a clear understanding of the flood hazard. The physical interpretation, highlighted by a global sensitivity analysis, showed precisely the dependence of the flood simulation on the main factors studied, i.e. the roughness coefficients and the characteristics of the breaches.

Keywords: flood hazard; dike breach; Monte Carlo framework; Global Sensitivity Analysis

1. Introduction

Floods may result from different phenomena, such as intense storms or prolonged rainfall, overloaded drainage systems, overtopping or failure of defense structures (e.g. levees, dams), and storm surges. Worldwide, they have unfortunately become a common experience, inflicting massive losses on human life and widespread destruction of properties and environment. Between 1980 and 2020, approximately 40% of total economic losses in European Environment Agency member countries are attributable to hydrological events [1]. Costs and causalities are likely to be exacerbated owing to the effects of population growth and living standards, climate change, increased urbanization, limited drainage infrastructures and storage zone [2-3-4], as well as to the actual limitations of early warning systems. The European Flood Directive 2007/60/EC demands all member states to produce flood hazard assessment and mapping for their territory. To cater for this demand, multidisciplinary frameworks for flood resilience [5-6] have been carried out (e.g., FLOODsite [7]; FloodProBE [8], [9]). The present study focuses on the numerical simulation of extreme floods exacerbated by the breaching of fluvial dikes (i.e. embankment levees along river banks).

Fluvial dikes have been built to channelize the flow, limit the lateral riverbed migration, or as defense structures against floods. Most of the levees are made of heterogeneous material making the analysis of their safety difficult in view of the multiplicity of scenarios responsible for their failure and the strong uncertainties on the underlying mechanisms [10]. Dike breaches can be induced by different phenomena but overtopping/overflow of a levee can induce major damages linked to external erosion, especially on the landside

 doi:10.20944/preprints202210.0474.v1

slope [11]. Overtopping occurs typically if the water level in the river exceeds the dike crest. Due to the well-known "levee effect", flood-prone areas are overused by population and industrial activities [12]. Quantitative flood hazard assessment is an important part of the effort toward gaining higher safety levels of flood-prone areas, identifying possible hazards, and analyzing their causes, frequencies, and uncertainties [13]. Numerical hydraulic models for flood propagation induced by levee breaches do not only offer the potential to characterize flow and to map flood hazard, but also help to design mitigating measures and support effective land use and emergency planning [14].

Flood modelling tools allow replicating past events, assessing the current inundation state and predicting likely futures with an uncertainty range that is strongly linked to the approximate description of hydraulic parameters [15], meteorological and geographical data [16-17], and to the breach parameters (e.g. location, condition for initiation, expansion, final dimensions [18-19-20-21-22]). Despite the significant improvement in computational resources and the accuracy of numerical models, the turbulent nature of fluid mechanics equations, combined with the uncertain model inputs and parameters, limit the performance of hydraulic modelling. The need for realistic hydrodynamic flow simulations cannot be satisfied with deterministic forecasts, thereby calling for model uncertainty quantification. Parameters that are often unknown or difficult to assess include defense structure failure, topography, bed friction, and hydrological forcing. In this work, the topography and hydrological forcing are considered as known. Integrating topography in an uncertainty quantification process is challenging, due to the spatial structure characterization of its uncertainty in relation to the river/channel morphology [23]. The upstream boundary condition corresponding to the hydrological forcing is extrapolated from discharge frequency curves. A stage-discharge relationship reconstructed from hydrological observations is assumed to be known at the model downstream end, although, in addition to measurement errors, this relationship relies on several assumptions (e.g. uniform flow), some of which inevitably introduce errors [24].

For the sake of simplification, the present work focuses on how the friction parameter and the occurrence of multiple breaches influence the flood hazard assessment. The same methodology can be applied for other uncertain parameters.

Bed roughness is considered as primary source of uncertainty as it is used to compensate some omitted physical processes [25]. The levee breach modelling ranges from simple empirical equations [26] to complex models solving coupled system of shallow water equations and sediment transport formula [27]. For practical modelling of flood inundations caused by overtopping flows induced levee breaching, parametric breach models are a suitable approach [28], describing the breach expansion by simplified equations. Since breach behavior is highly dependent on the geometrical and geotechnical characteristics of the levee, there are uncertainties with regards to the breach initiation and development processes [29].

Probabilistic approaches have gained attention for providing insight into the robustness of the modelling results. The most classical method to propagate uncertainty through the model is the Monte Carlo technique [30-31-32]. Monte Carlo methodology is generic and robust, but computationally expensive and can be prohibitive for the flow simulation of large river domains with complex topographies [33]. One way to lower the computational burden is to use simplified one-dimensional (1D) or coupled 1D with 2D depth-averaged numerical models. However, 1D models are not really able to represent some aspects of out-of-bank flows, such as the complex topographic gradients found in floodplains or confluence areas. Coupled 1D-2D models can be a good alternative to 2D models [34], but the exchange of flows between 1D and 2D models are often subject to limitations (e.g. momentum exchange between channel and floodplain or return flow from floodplain back to channel are ignored) [35]. Two-dimensional (2D) depth-averaged hydraulic models are currently at the forefront of engineering application for river flood inundation prediction [36].

Based on a reduced number of model computations, other effective ways of overcoming the large Monte Carlo computational burden can be found in literature. First, an

 doi:10.20944/preprints202210.0474.v1

alternative known as emulation modelling aims at representing the large-scale flood hazard system with a model that is much less computationally demanding [37]. Unfortunately, the emulator techniques introduce additional uncertainties, as they approximate the original model. Second, the associated probabilities for a design flood event of given return period are estimated from breach scenario probabilities derived, for instance, from fragility curve [33]. However, computational effort can drastically increase with the number of multiple breaches considered [38].

This work presents a flood hazard assessment study over a reach of the Loire river. A 2D depth-averaged inundation model is used to assess the impact of multiple dike failures induced by flow overtopping for different flood events (from 100 to 1000-year return periods). Considering the presence of multiple levee breaches is not so widespread [38]. The uncertainties regarding final width breach development and breach initiation conditions as overtopping level with a sufficient energy balance (water-level difference between upstream and downstream of the breach) are considered here. Finally, although the flood simulation can be sensitive to the roughness coefficients and breach characteristics [39], to the best of our knowledge, a probabilistic flood hazard study tackling these uncertainties is still missing. In this work, the Monte Carlo method is used to propagate the uncertainty through the hydrodynamic model.

The results are analyzed twofold: on one hand, a global statistical analysis all over the domain is done to provide flood inundation maps. On the other hand, the effect of variability of random inputs is assessed at some specific points (around a heavily populated area, for example). In this study, we are in the presence of a high-dimensional uncertain input space (approximatively 300 uncertain parameters), therefore a special attention has been paid to perform a relevant sensitivity analysis to clearer understand, in depth, the relationship between the uncertain parameters and the simulated state variables. This is another significant contribution of the current work.

The paper is organized as follows: Section 2 describes the application case and the numerical model used. Section 3 presents the uncertainty framework. Section 4 describes the uncertainty quantification study results. Section 5 is the discussion, followed by concluding remarks in Section 6.

2. Case study and numerical model

The flood hazard assessment is conducted with a 2D depth-averaged hydraulic model (i.e. shallow water equations) on a reach of the Loire river (France). The study area extends between St-Martin-sur-Ocre (upstream) and Châteauneuf-sur-Loire (downstream), that is a reach of about 50 km long (Figure 1-(a)). Levees and longitudinal weirs were progressively built since the 19th century to protect population and assets against floods of the Loire river. In the present work, eight breaches are considered, five being located at the right side and three at the left side of the river.

2.1. Model set up

The 2D depth-averaged hydrodynamic model TELEMAC-2D, from the TELEMAC-MASCARET hydro-informatic system (www.opentelemac.org), is used to simulate free-surface flow using the finite element method on a triangular element mesh [40]. TELEMAC-2D has been widely applied for simulating flood propagation induced by levee breaching [28-41]. The mesh composed of 311,112 nodes is elaborated from breaklines so that topographic singularities (e.g. roads, dikes, weirs, low walls, etc.) could be accurately described. The grid size varies from 10 to 20 m in the sectors with topographic singularities and steep slopes (e.g. main bed, levees, etc.) to more than 350 m at the edge of the valley (Figure 1-(b)). The densely urbanized regions are numerically considered through specific friction areas. A constant flow discharge is imposed at Saint-Martin-sur-Ocre, whereas a stage-discharge relationship (measurements at gauge station at Châteauneuf-sur-Loire) is defined as downstream boundary condition.

Preprints (www.preprints.org) | NOT PEER-REVIEWED | Posted: 31 October 2022 doi:10.20944/preprints202210.0474.v1

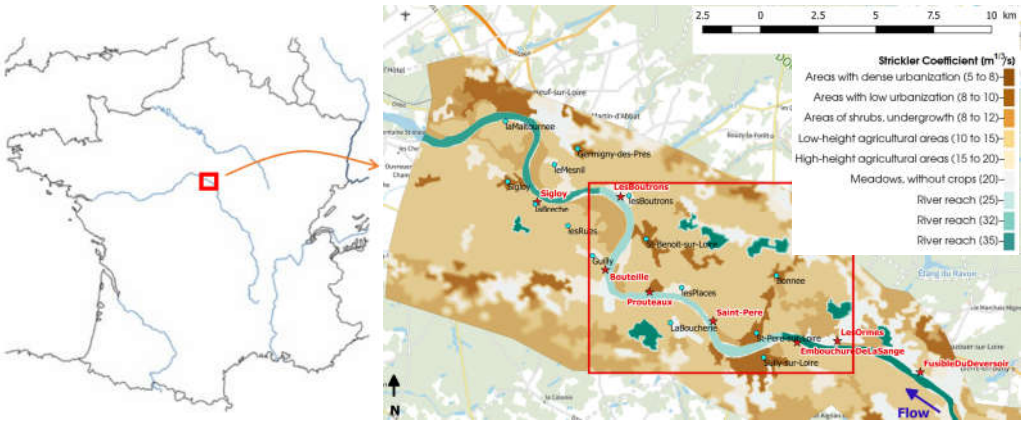

(a)

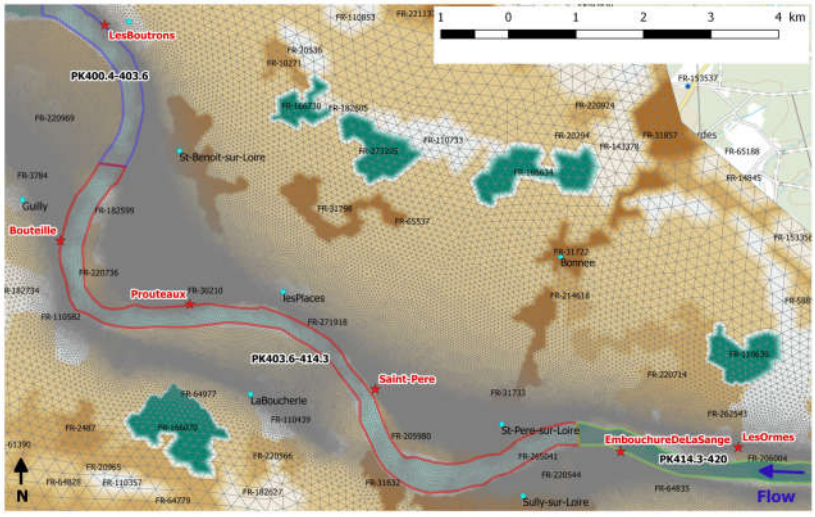

(b)

Figure 1. Study area: (**a**) domain of interest; (**b**) zoom area. Red stars indicate breach locations (weak points of the levee) and blue dots are points of interest located in floodplain. Colored surfaces correspond to friction coefficient areas. Range of variation of friction coefficients in floodplain is reported in the legend.

2.2. Hydrodynamic model

TELEMAC-2D solves the following shallow water equations (Equations (1)-(3)).

$$\frac{\partial h}{\partial t} + \frac{\partial}{\partial x}(hu) + \frac{\partial}{\partial y}(hv) = 0 \quad (1)$$

$$\frac{\partial hu}{\partial t} + \frac{\partial}{\partial x}(huu) + \frac{\partial}{\partial y}(huv) = -gh\frac{\partial Z_s}{\partial x} + hF_x + \nabla\left(hv_e\nabla(u)\right) \quad (2)$$

$$\frac{\partial hv}{\partial t} + \frac{\partial}{\partial x}(huv) + \frac{\partial}{\partial y}(hvv) = -gh\frac{\partial Z_s}{\partial y} + hF_y + \nabla\left(hv_e\nabla(v)\right) \quad (3)$$

where x and y are horizontal Cartesian coordinates; t is time; u and v are components of the depth-averaged velocity in x - and y -direction, respectively; h is the water depth; v_e is an effective diffusion representing depth-averaged turbulent viscosity v_t and dispersion; Z_s is the free surface elevation; g is gravitational acceleration; F_x and F_y refer to the friction forces in x - and y -direction, respectively (Section 2.2.1). TELEMAC-2D has been validated for many analytic, experimental and real-world cases [42]. In this work, the finite element approach is used to solve the previous equation system. The N

Preprints (www.preprints.org) | NOT PEER-REVIEWED | Posted: 31 October 2022 doi:10.20944/preprints202210.0474.v1

edge by edge scheme (NERDS) and the Positive Streamwise Invariant (PSI) distributive scheme are used for solving the advection of velocity and water depth, respectively. Wetting and drying of grid elements is considered through a correction of the free surface gradient [40].

2.2.1. Roughness coefficient

The following component of the friction force are treated in a semi-implicit form within TELEMAC-2D [40]:

$$\begin{cases} F_x = -\dfrac{u}{2h} C_f \sqrt{u^2 + v^2} \\ F_y = -\dfrac{v}{2h} C_f \sqrt{u^2 + v^2} \end{cases} \quad (4)$$

where C_f is a dimensionless friction coefficient. Empirical formulas are used for calculating C_f [43]. In the present work, the following Strickler formula is used, in which the Strickler coefficient K_s is a parameter to be calibrated:

$$C_f = \frac{2g}{{K_s}^2 h^{1/3}} \quad (5)$$

The model calibration is a reverse method which is used to find an "acceptable" friction coefficient leading to computed water levels close to the measured ones for a given flow discharge. In the present study, the Strickler coefficient is assumed constant in time and spatially distributed. Three events are retained from Banque HYDRO data [44] (December 2003 (3,320 m³/s at Given, 17-year flood), January 2008 (890 m³/s at Given, less than 1-year flood) and November 2008 (2,320 m³/s at Given, 4-year flood)) for calibration of the main river Strickler coefficients. Observation data are unavailable in the floodplain, and no significant flooding events have been recorded to date. Thus, the floodplain friction areas are identified based on the inventory of Corine Land Cover of 2018 [45]. For each area and following expert knowledge, the Strickler coefficient is taken as the mean value of an interval bounded by physical values depending on soil occupation.

2.2.2. Levee breaches

Simplified models describe the levee breaching by making assumptions on the location, initiation, development, number, and shape of the levee breach, often based on engineering experience, and knowledge of historical events [28]. In the present study, breaches are initiated at pre-defined locations (Figure 1-(a)), identified from historical observations [46-47] and field survey. The breach initiation occurs if the overtopping flow depth above the dike (E_s) reaches a threshold value and when the energy balance (ΔE), defined as the difference between the upstream head (channel side, E_{riv}) and downstream head (floodplain side, E_{pla}) of a weak point is high enough (Figure 2).

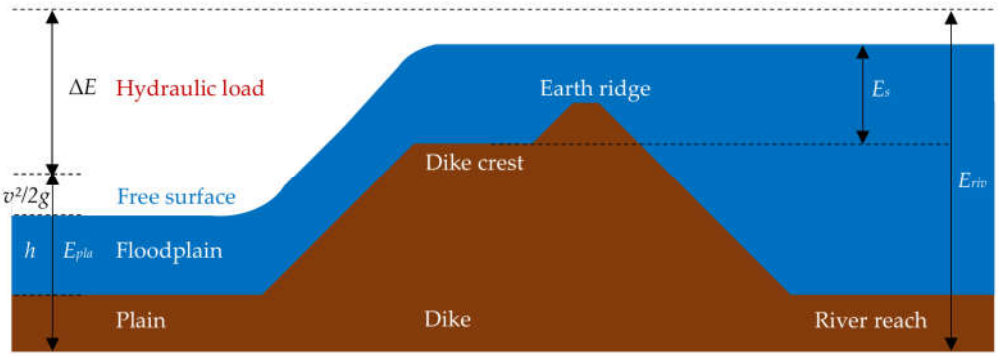

Figure 2. Scheme illustrating variables used to identify initiation of breach expansion on a profile across a levee (surmounted by an earth ridge). v (m/s) is mean flow velocity.

Preprints (www.preprints.org) | NOT PEER-REVIEWED | Posted: 31 October 2022 doi:10.20944/preprints202210.0474.v1

Current state-of-the-art on the breaching of fluvial dikes due to overtopping flows shows that the breaching expansion is progressive (i.e. non-instantaneous) [48-49], following two main phases (referred to as breach formation and development, respectively). During the first phase, the breach deepening (vertical incision of the breach) is faster than breach widening [10]. Then, when the breach bottom reaches the foundation of the dike or a non-erodible layer, only lateral widening is observed until the breach stabilizes (i.e. fully formed breach with erosion being stopped). For the sake of simplification, we assume that the breach shape is rectangular, and its expansion follows one phase according to this linear law:

$$B(t) = k_{in} \times t, \forall\, t \leq T_f\ . \tag{6}$$

where t is time in hours (after breach initiation), B is the breach width in meters at time t, k_{in} (m/h) is the breach widening rate, assumed constant in this study, and T_f is the total duration of the breach expansion.

The breach time-deepening is also described according to a linear law:

$$Z_b(t) = Z_b(0) - \frac{Z_b(0) - Z_{b,min}}{T_d} \times t, \forall\, t \leq T_d\ . \tag{7}$$

where, Z_b is the breach invert elevation at time t, $Z_b(0)$ is the breach invert initial elevation, $Z_{b,min}$ is the breach minimum level, and T_d is the breach deepening duration. Since the breach deepening is evolving faster than the breach widening, T_d is taken 10 times smaller than T_f.

3. Uncertainty assessment methodology

Here below we describe the methodology used for assessing how the friction parameter and multiple breaches influence the flood hazard evaluation. The methodology involves three steps: (i) uncertainty quantification, (ii) uncertainty propagation, and (iii) sensitivity analysis. The Application Programing Interface (API) framework described by Goeury et al. [50] was used. The chart of the methodology is shown in Figure 3.

3.1. Uncertainty quantification

3.1.1. Flood inundation scenarios

Extrapolated flow discharges from frequency curves of 100-, 200-, 500- and 1000-year return period scenarios, respectively, are used as the upstream boundary condition. A real duration of four days is simulated, with a time step of 2 s, requiring one and a half hours of parallel computation with Intel-Xeon(R) Platimum 8260 processors. The quantity of interest is the flow depth at the steady state condition.

3.1.2. Uncertain parameter characterization

- Roughness coefficient quantification:

Following the principle of maximum entropy, a uniform distribution for the roughness coefficient is imposed. Uniform bounds in riverbed are set to ± 2.5 $m^{1/3}s^{-1}$ from the calibrated value to be compatible with the calibration accuracy of 20 to 25 cm. In the floodplain, bound values are assigned according to land cover classes (Table 1). A total of 280 friction areas are considered.

Preprints (www.preprints.org) | NOT PEER-REVIEWED | Posted: 31 October 2022 doi:10.20944/preprints202210.0474.v1

Table 1. Floodplain roughness characterization and associated probabilistic distribution.

Land cover class	Variation interval ($m^{1/3}s^{-1}$)	Probability distribution
Areas with dense urbanization	[5 , 8]	Uniform
Areas with low urbanization	[8 , 10]	
Areas of shrubs, undergrowth	[8 , 12]	
Low-height agricultural areas	[10 , 15]	
High-height agricultural areas	[15 , 20]	

- Dike breach controlling coefficient quantification:

The uncertain breach parameters considered in this study are the initiation criteria and the final breach width (Table 2).

Table 2. Breach parameters with associated range of variations defined by expert knowledge.

Name	Dike crest $Z_b(0)$ (m NGF N)	Failure criterion E_s (m)	Failure criterion ΔE (m)	Final breach width B_f (m)	Dike material
Fusible du déversoir	120.80	[−0.25 , 0.3]	[0.3 , 1.5]	[50 , 850]	clay-dominated
Les ormes	119.72	[0.05 , 0.6]	[0.3 , 1.5]	[50 , 950]	sandy-loamy
Embouchure de la Sange	118.82	[0.05 , 0.6]	[0.3 , 1.5]	[50 , 950]	sandy-loamy
Saint-Père	116.66	[0.05 , 0.6]	[0.3 , 1.5]	[50 , 950]	clay-dominated
Prouteaux	115.60	[−0.25 , 0.3]	[0.3 , 1.5]	[50 , 950]	sandy-loamy
Bouteille	114.46	[−0.25 , 0.3]	[0.3 , 1.5]	[50 , 950]	sandy-loamy
Les Boutrons	112.08	[0.05 , 0.6]	[0.3 , 1.5]	[50 , 950]	sandy-loamy
Sigloy	111.54	[0.05 , 0.6]	[0.3 , 1.5]	[50 , 950]	sandy-loamy

The breach triggering is assumed to occur at the lowest elevation point of the levee crest determined from topographic data (Lidar or survey data). Failure by overtopping (*Failure Criterion* E_s) is allowed in a certain range of variation to take into consideration the topographic measurement uncertainty (minimum permitted values: -0.25 m and 0.05 m respectively for Lidar data and accurate topographic surveys) and geotechnical characteristics of the levee (for instance, Loire river levees typically feature a "banquette" (earth ridge) on top [51] (Figure 2) providing additional resistance to the levee characterized by a highest maximal value (0.6 m) in comparison to a dike without earth ridge (0.3 m)). The energy balance criterion ΔE is set, following expert opinion, to $[0.3 , 1.5]$ (m). The duration of overtopping over the dike crest is not considered in this study since its quantification is subject to significant uncertainty for a relatively low potential impact [22].

The breach shape is assumed rectangular, characterized by its final width (B_f), widening rate (k_{in}) and final invert elevation ($Z_{b,min}$). The minimum and maximum values of the final breach width interval ($[50 , 950]$ (m)) are determined from historical analysis [46] and geotechnical considerations [47]. The breach widening rate k_{in} is considered constant, with values of 102 m/h and 10.2 m/h corresponding to, predominantly sandy-loamy and clay-dominated structures, respectively [52-53-54]. The duration of breach widening T_f is also assumed deterministic and deduced from Eq. (6) using B_f and k_{in}. The breach depth is assumed to be the same as the height of the levee itself, as non-erodible layers is considered in dike foundations.

3.2. Uncertainty propagation

To handle dynamic system behavior under parameter uncertainty, a set of sample configurations is generated using random sampling. In the sampling procedure, the parameter uncertainties are taken in a uniform distribution whose limits are defined by the minimum/maximum values of its variation range. The solver TELEMAC-2D (thereafter denoted M) ensures the relationship between a configuration vector of model uncertain inputs $\boldsymbol{\theta}^j = \left(\theta_{j,1}, \theta_{j,2} \cdots \theta_{j,v}\right)$ and the output quantity of interest $Y(\mathbf{x})$ whereby $Y(\mathbf{x}) =$

Preprints (www.preprints.org) | NOT PEER-REVIEWED | Posted: 31 October 2022 doi:10.20944/preprints202210.0474.v1

$M(\boldsymbol{\theta}^j, \mathbf{x})$ (Figure 3). As TELEMAC-2D is a spatially discrete model, for a realization $\boldsymbol{\theta}^j$, the model output $\mathbf{Y}$ is composed of scalar output given on a set of $m \in \mathbb{N}$ space coordinates $\{\mathbf{x}_1, \ldots, \mathbf{x}_m\}$ such as $\mathbf{Y} = (Y_1, \ldots Y_m)$ (with $Y_i = Y(\mathbf{x}_i) = M(\boldsymbol{\theta}^j, \mathbf{x}_i)$). The full set of spatially discrete output over the complete random sampling gives a matrix of size $n \times m$ (where n is the number of Monte Carlo simulations).

$$\mathcal{Y} = (\mathbf{Y}_1, \ldots, \mathbf{Y}_m) = \begin{pmatrix} y_{1,1} & y_{1,2} & \cdots & y_{1,m} \\ y_{2,1} & y_{2,2} & \cdots & y_{2,m} \\ \vdots & \vdots & \ddots & \vdots \\ y_{n,1} & y_{n,2} & \cdots & y_{n,m} \end{pmatrix} \tag{8}$$

Each row of the matrix $\mathcal{Y}$ corresponds to the flow depth throughout the computational domain for a fixed upstream flow scenario of uncertain input parameter. From matrix $\mathcal{Y}$, statistical estimators can be calculated, such as first two statistical moments (i.e., mean and variance values) of the response quantity at a spatial coordinate. The Monte Carlo method is robust with a convergence rate, $O(\sqrt{n})$, that is independent of dimension, i.e. the number of factors (v) in the problem.

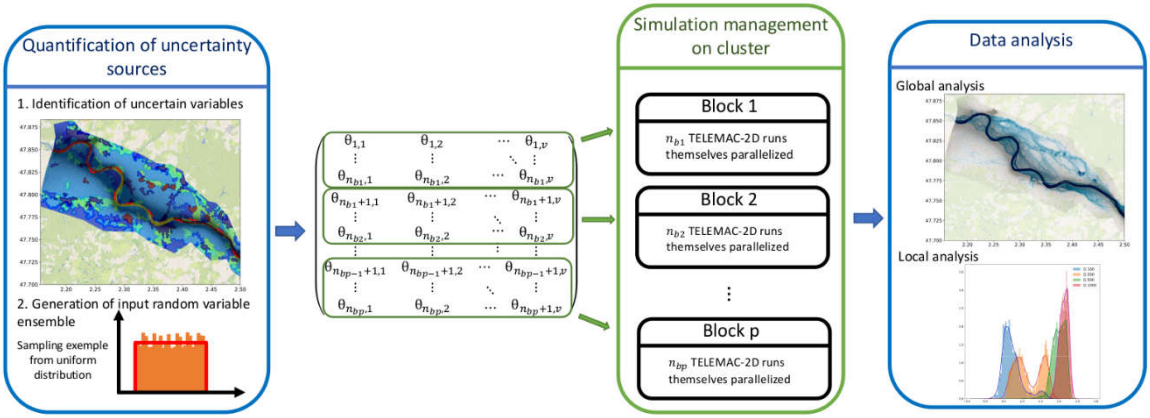

Figure 3. Overview of Monte Carlo framework.

3.3. Sensitivity analysis

The sensitivity analysis aims at quantifying the impact of uncertainty in input variables on the accuracy of the model output variables. Conventional approaches to Global Sensitivity Analysis (GSA) imply the stochastic estimation of statistical moments [55], and indices are classically achieved with the Monte-Carlo technique [56]. To alleviate the computational burden of Monte Carlo approach, emulators can be used to estimate sensitivity indices [57]. However, the non-linearity of local phenomena, such as dike overtopping, may affect only a small proportion of input parameter space and leads to output variability that is difficult to translate by any moment of the random variable. This can lead to uncertainty in the determination of sensitivity [58]. To obtain accurate results, sensitivity analysis must satisfy the following requirements [59-60]: global (i.e. entire input distribution taken into consideration), model free (i.e. no assumptions on the model functional relationship to its inputs), moment independence (i.e. avoid some information loss by the use of an output variability summary) and be quantitative. In this framework, two statistical moment independence and model free GSA methods are carried out: a permutation feature importance based on a model training with machine learning and the statistical Borgonovo moment-independent sensitivity measures [60]. For the sake of clarity, in the following, the GSA methods are described in the case of scalar output such as $Y_p = Y(\mathbf{x}_p) = M(\boldsymbol{\theta}^j, \mathbf{x}_p)$ where $\mathbf{x}_p$ is the location of the variable of interest.

3.2.1. Permutation feature importance

The permutation feature importance consists of measuring the decrease in the prediction score in a machine learning algorithm after permuting randomly an input parameter (a feature) [61]. Randomly re-ordering a parameter causes a prediction deterioration

Preprints (www.preprints.org) | NOT PEER-REVIEWED | Posted: 31 October 2022 doi:10.20944/preprints202210.0474.v1

that indicates how much the model depends on the feature. If the decrease in prediction quality is small or high, the model is little or very sensitive to the shuffled input parameters. In this study, the prediction score is the coefficient of determination R^2, and Random Forest algorithms [61] are employed as machine learning regressors since they do not make any assumptions on the model functional relationship to its inputs.

Random forests are built by averaging the prediction of many individual decision trees. Each decision tree is fitted to a bootstrap sample created from the learning dataset (sampling matrix $\mathcal{D} = (\boldsymbol{\theta}_1, \boldsymbol{\theta}_2, \dots, \mathbf{Y}_p)$). A decision tree is a recursive process of splitting internal nodes. To break-up a node, a collection of candidate splits is generated, and a criterion is evaluated to choose between them. For each candidate split $s = (k, T_{val})$, the data are routed to subtrees depending on whether it exceeds the threshold value T_{val} in the chosen dimension k such as:

$$\begin{cases} \mathfrak{C}_l = \{(\boldsymbol{\theta}_1, \boldsymbol{\theta}_2, \dots, \mathbf{Y}_p) | \theta_{\boldsymbol{k}} \leq T_{val}\} \\ \mathfrak{C}_r = \{(\boldsymbol{\theta}_1, \boldsymbol{\theta}_2, \dots, \mathbf{Y}_p) | \theta_{\boldsymbol{k}} > T_{val}\} \end{cases} \tag{9}$$

Then, the variance reduction method is used to determine the optimal split at each node of the decision tree. This method is based on a calculation of the following equation:

$$\max_{s} \left(\sum_{y_i \in \mathfrak{P}} \frac{\left(y_i - \overline{y^{\mathfrak{P}}}\right)^2}{n_p} - \frac{n_l}{n_p} \sum_{y_i \in \mathfrak{C}_l} \frac{\left(y_i - \overline{y^{\mathfrak{C}_l}}\right)^2}{n_l} - \frac{n_r}{n_p} \sum_{y_i \in \mathfrak{C}_r} \frac{\left(y_i - \overline{y^{\mathfrak{C}_r}}\right)^2}{n_r} \right) \tag{10}$$

where $\mathfrak{P}$ denotes the parent node containing n_p training samples, $\mathfrak{C}_l$, $\mathfrak{C}_r$ are respectively the left and right child node subtrees containing respectively n_l, n_r data, and $\overline{y^{\mathfrak{x}}}$ is the mean value of output values in the node $\mathfrak{x} \in \{\mathfrak{P}, \mathfrak{C}_l, \mathfrak{C}_r\}$.

The terminal nodes of a tree, also called leaf nodes, provide the final prediction by averaging the output of training samples within the corresponding leaf node. The methodology described here before was performed based on an open-source library for Machine Learning named "scikit-learn" [62].

3.2.2. Borgonovo sensitivity analysis

Moment-independent sensitivity measures overcome the output variability summary associated with the interpretation of variance-based measures. In this framework, a sensitivity measure based on the shift between the output distribution and the same distribution conditionally to a parameter was proposed [60] and reads as:

$$\delta_i = \frac{1}{2}\left[\int \pi_{\Theta_i}(\theta_i) \left[\int \left|\pi_Y(y) - \pi_{Y|\Theta_i}(y)\right| dy\right] d\theta_i\right] \tag{11}$$

However, based on the entire distribution, the Borgonovo sensitivity analysis can become unsuitable when the computational cost of each run of the model is non negligible or the number of model inputs is large. Thus, a sample-based estimation was proposed to handle this issue [63]. In the present work, this Borgonovo sensitivity analysis was carried out based on an open-source library for performing sensitivity analyses "SALib" [64].

4. Results

Separated and identifiable Monte Carlo simulations were performed based on the MPI parallel computing technology for launching and managing the TELEMAC-2D solver computations (Figure 3). A sample set of size n =3,000 is set for the uncertainty propagation. This number was determined based on a convergence study carried at some control points (see Section 4.2). The obtained results are analyzed twofold: on one hand, a global statistical analysis on the whole domain is performed. On the other hand, the effect of the variability of the random inputs is assessed at some specific points (selected around a populated area, for example, as reported in Figure 1).

4.1. Global statistical analysis

Preprints (www.preprints.org) | NOT PEER-REVIEWED | Posted: 31 October 2022 doi:10.20944/preprints202210.0474.v1

4.1.1. Uncertainty propagation

Figure 4 shows the probabilistic flood hazard maps of the 90th percentile water depths. These results could be of importance for flood management by identifying water surface elevations and lateral flood extents for each flood event. As expected, the 90th percentile water depth level increases with the rise in the flood return period. To better analyze the lateral flood extents, the 90th percentile scalar flow velocity calculated for different flood events of different return periods is also computed and presented in Figure 5.

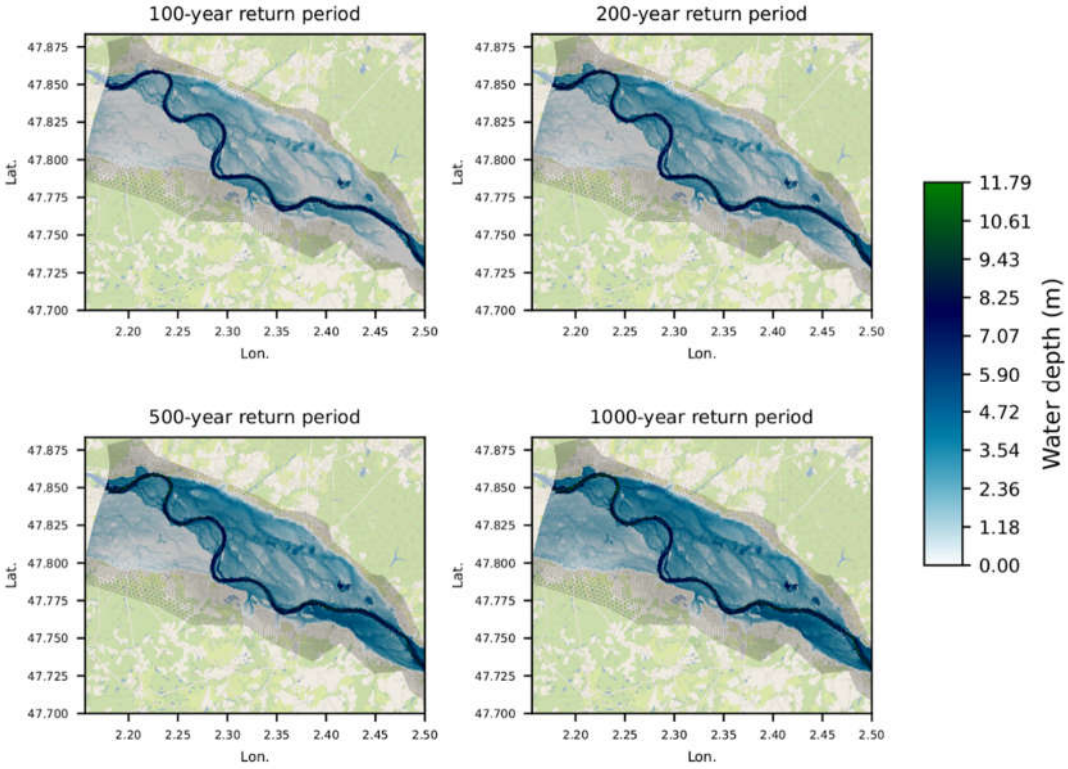

Figure 4. Probabilistic inundation extent map of 90th percentile water depths for 100, 200, 500 and 1000-year return period floods.

Preprints (www.preprints.org) | NOT PEER-REVIEWED | Posted: 31 October 2022 doi:10.20944/preprints202210.0474.v1

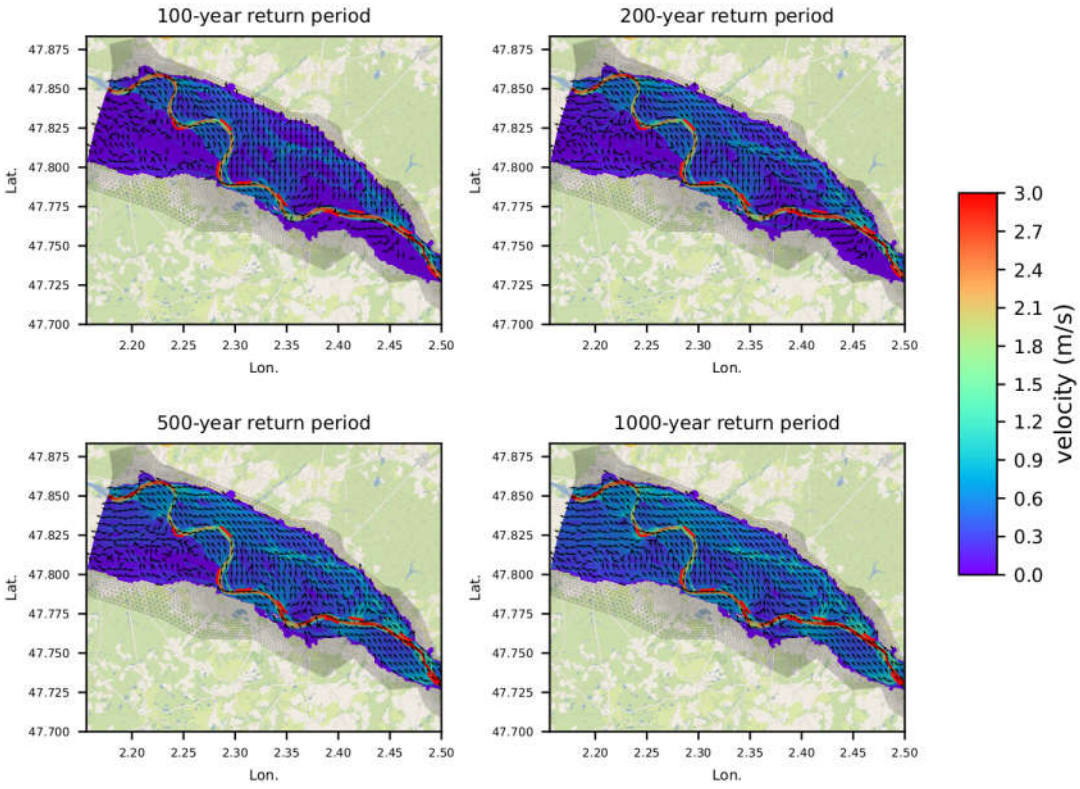

Figure 5. Probabilistic inundation map of 90th percentile flow scalar velocity with velocity vectors for 100, 200, 500 and 1000-year return period floods with location of potential dike breach (—).

It can be noticed that not all dike breaches are formed for the different scenarios. The water elevation in the right floodplain is directly influenced by the *Fusible du déversoir*, *Saint-Père* and *Les Boutrons* levee breaches (Figure 1) which occur from the 100-year return period flood event. On the other hand, the significative rise in water elevation in the left floodplain occurs at high flood event scenarios with *Embouchure De La Sange* and *Sigloy* levee breaches (Figure 1). As a result, in terms of flood mitigation, it is imperative that hazard related to levee systems are thoroughly evaluated.

4.1.2. Sensitivity analysis

For a given flood scenario, the breach width can significantly affect the water heights in the floodplain since it is a parameter influencing on the breach outflow hydrographs [20]. Figure 6 shows the computation of the Borgonovo index to evaluate the influence of a breach width on the water depth. Particularly, a value close to 0 and conversely 1 means the output is, respectively, independent or highly dependent on the variable of interest. Figure 6 highlights the spatial influence scale and intensity of the *Saint-Père* breach width uncertain variable on the water depth. The intensity of the parameter influence increases with increasing flood scenarios discharge. This increase is accompanied by a more localized spatial effect, emphasizing the need for local flood analysis to better understand the conditions under which flood mitigation is most likely to occur, thereby helping to make communities more resilient to flooding [65].

Preprints (www.preprints.org) | NOT PEER-REVIEWED | Posted: 31 October 2022 doi:10.20944/preprints202210.0474.v1

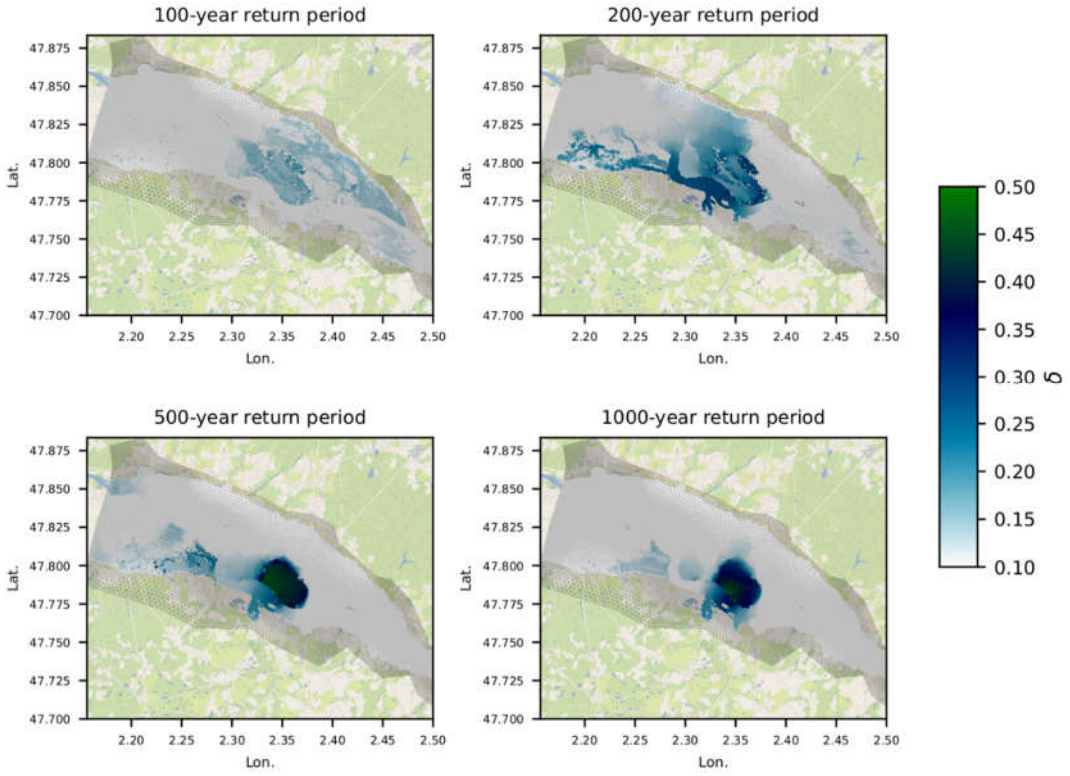

Figure 6. Borgonovo indices for *Saint-Père* breach width for 100, 200, 500 and 1000-year return period flood events.

4.2. Local statistical analysis

4.2.1. Uncertainty propagation

A statistical analysis of flow depth values at specific locations yields a valuable tool for understanding the flooding patterns. When applying a sampling-based statistical analysis, the estimators are not computed exactly but rather approximated from the available samples. The robustness and convergence of such estimates should be assessed. To address this issue, the convergence rates of the dispersion coefficient (ratio of the standard deviation to the mean) and its 90% confident interval obtained by the bootstrap method are evaluated as the sample size n increases. As illustrated for selected locations in Figure 7, the number of samples needed to reach stable statistical estimates can vary from one discharge to another. However, from a sample size of 2,500, the statistical estimators are stabilized. The number of 3,000 model evaluations considered in this study is satisfactory to obtain reliable results.

Preprints (www.preprints.org) | NOT PEER-REVIEWED | Posted: 31 October 2022 doi:10.20944/preprints202210.0474.v1

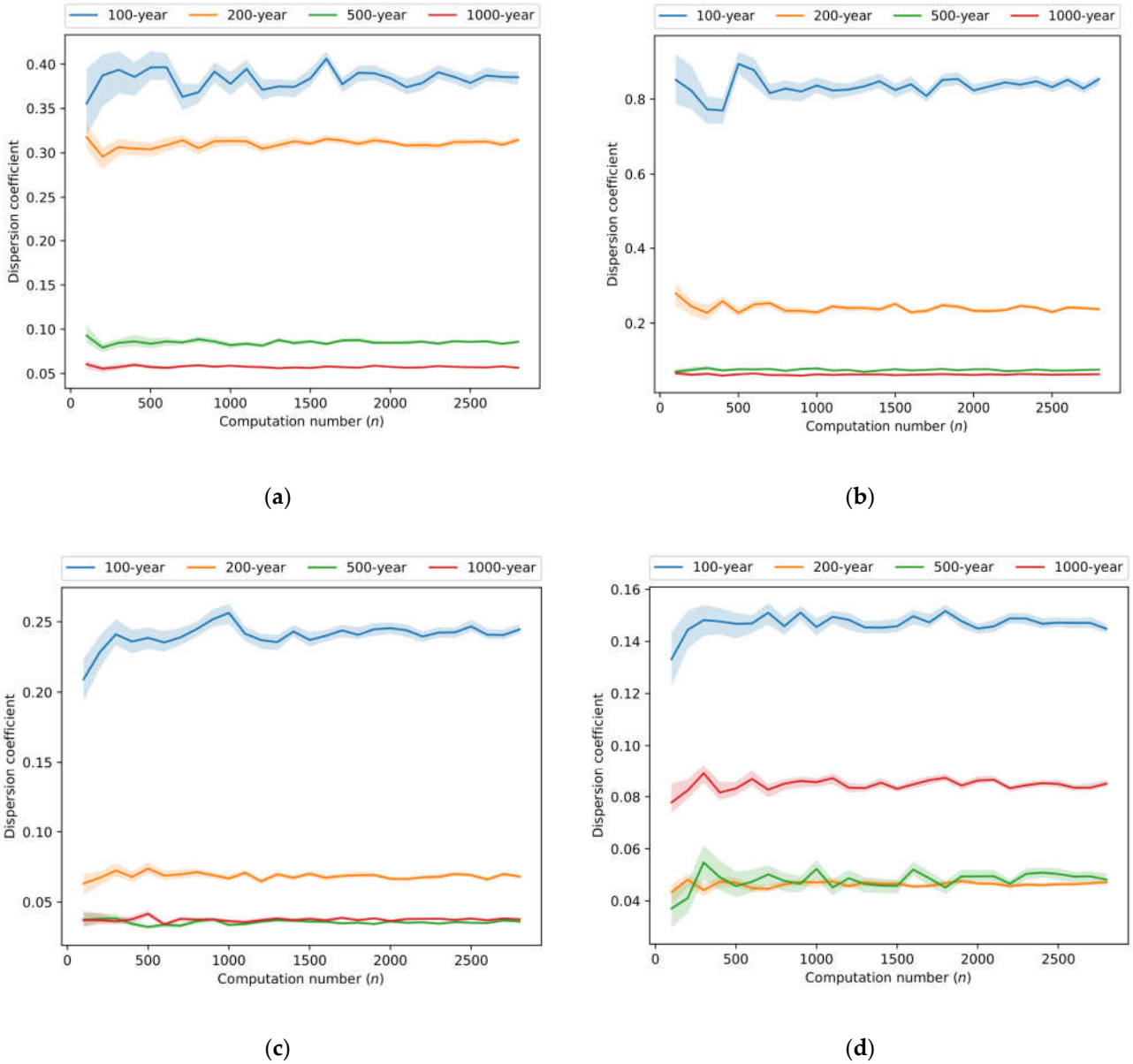

Figure 7. Convergence graphs of dispersion coefficient and its 90% confident interval for 100, 200, 500 and 1000-year return period flood scenarios at some control points: (**a**) Sully-Sur-Loire; (**b**) Les Places; (**c**) Les Boutrons; (**d**) Le Mesnil.

Figure 8 displays how the model parameter uncertainties (roughness coefficients and levee breach characteristics) affect the water depth at selected locations for given flood scenarios. The spreading of the water depth distribution is more significant for low flood scenarios (100-year return period) and diminishes with the rise in the flood discharge. This demonstrate that high flood scenarios are less sensitive to the selected uncertain parameters. The results highlight the complexity of the flow with non-symmetric (non-Gaussian) water level distributions. Some water level distributions show multiple peaks in the PDF, especially for low flood scenarios. These multimodal distributions indicate that the control point sample can have several patterns of response, suggesting that the flooding patterns can drastically change starting from a given combination of the uncertain inputs.

Preprints (www.preprints.org) | NOT PEER-REVIEWED | Posted: 31 October 2022 doi:10.20944/preprints202210.0474.v1

4.2.2. Sensitivity analysis

Table 2 summarizes the sensitivity results at Les Places control point. The sensitivity analysis methods tested in this work lead to a similar ranking of importance of the uncertain parameters. This statement, in contrast to the work presented in [58], confirms the requirement for sensitivity analysis (global, model free, moment independence and be quantitative) to produce accurate results. Of all the uncertain input parameters, only several (levee breach parameters and roughness coefficient close to the point of interest) are identified as playing a major role in the accuracy of the water level at the relevant control point.

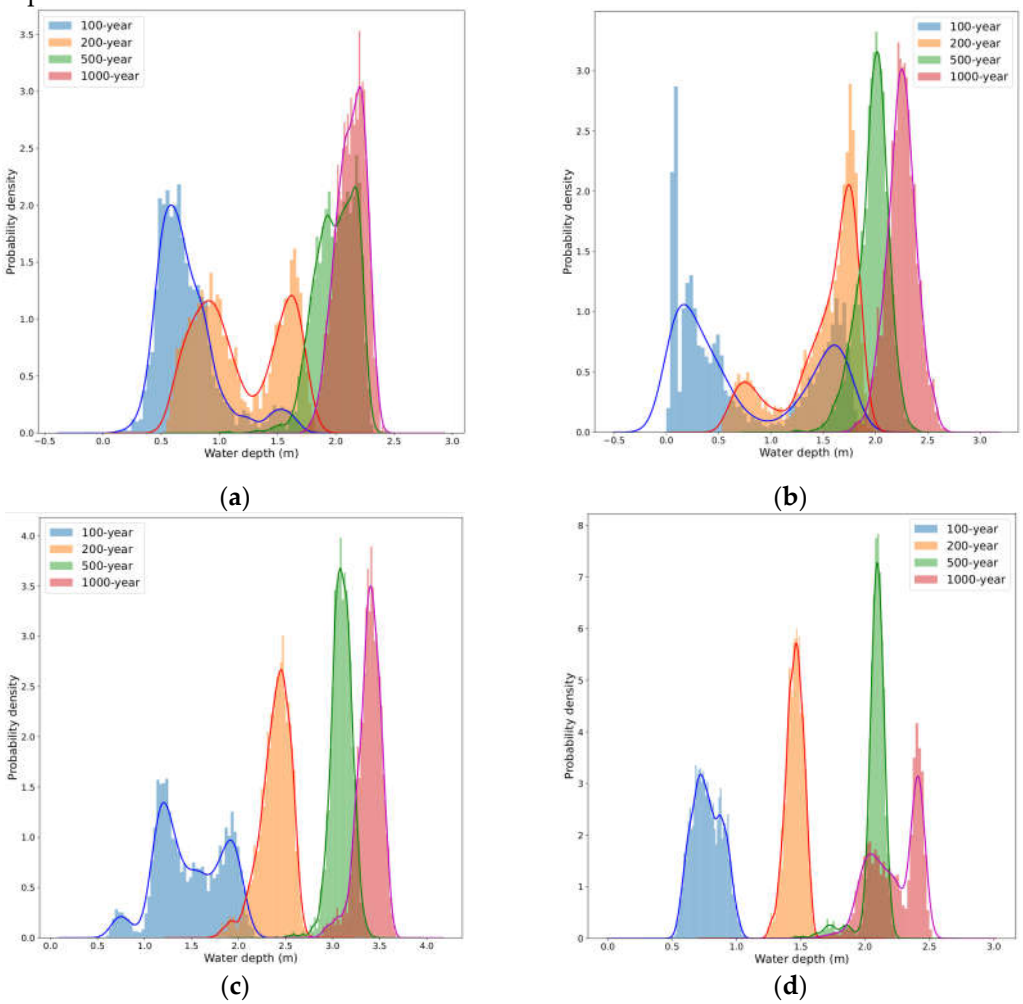

Figure 8. Water level Probability density function estimated with Monte-Carlo sampling for 100, 200, 500 and 1000-year return period floods at control points: (**a**) Sully-Sur-Loire; (**b**) Les Places; (**c**) Les Boutrons; (**d**) Le Mesnil.

Preprints (www.preprints.org) | NOT PEER-REVIEWED | Posted: 31 October 2022 doi:10.20944/preprints202210.0474.v1

Table 2. Sensitivity analysis at Les Places control point for 100, 200, 500 and 1000-year return period flood events: Borgonovo indices and permutation feature importance. PK and FR indicates, respectively, the friction coefficients for the riverbed and the floodplain (as reported in Figure 1).

Methods	Borgonovo indices	Permutation importance
100-years flood scenario	*Saint-Père* overtopping level: 0.22 *Fusible du déversoir* overtopping level: 0.20 PK403-414: 0.12 *Saint-Père* breach width: 0.10 *Fusible du déversoir* breach width: 0.091 FR-64977: 0.09	*Fusible du déversoir* overtopping level: 0.73 *Saint-Père* overtopping level: 0.72 PK403-414: 0.33 PK414-420: 0.099 *Saint-Père* breach width: 0.018 FR-64977: 0.0083
200-years flood scenario	*Saint-Père* breach width: 0.22 *Saint-Père* overtopping level: 0.21 PK403-414: 0.13 *Prouteaux* overtopping level: 0.097 FR-64977: 0.083 *Fusible du déversoir* breach width: 0.078	*Saint-Père* overtopping level: 0.91 PK403-414: 0.57 *Saint-Père* breach width: 0.24 FR-64977: 0.081 *Fusible du déversoir* breach width: 0.045 *Prouteaux* overtopping level: 0.01
500-years flood scenario	*Saint-Père* breach width: 0.32 FR-65537: 0.12 *Les Ormes* overtopping level: 0.085 *Prouteaux* overtopping level: 0.081 PK403-414: 0.071 *Les Ormes* breach width: 0.058	*Saint-Père* breach width: 1.12 FR-65537: 0.30 *Prouteaux* overtopping level: 0.14 *Les Ormes* overtopping level: 0.12 PK403-414: 0.048 *Prouteaux* breach width: 0.047
1000-years flood scenario	FR-65537: 0.22 *Saint-Père* breach width: 0.19 *Prouteaux* overtopping level: 0.10 PK403-414: 0.098 *Prouteaux* breach width: 0.062 *Les Ormes* breach width: 0.054	FR-65537: 0.68 *Saint-Père* breach width: 0.63 *Prouteaux* overtopping level: 0.23 PK403-414: 0.14 *Prouteaux* breach width: 0.10 *Les Ormes* breach width: 0.08

The physical interpretation of the sensitivity results allows a clearer understanding of the flood hazard. The concomitance of *Saint-Père* and *Fusible du déversoir* breaches could be at the origin of the bimodal behavior in the PDF observed for the 100-year return period flood scenario. In fact, the overtopping variables E_s and ΔE for initiation of these two breaches appear to be, with the same relative weight, the most important factors. The increase in flow rate is accompanied by a major impact of the *Saint-Père* breach width leading progressively to a single peak in the water depth distribution. These results are consistent with the physics of flow. In the case of a low flood event (100-year return period flood), overtopping level and bed roughness are of primary importance since they directly influence the initiation of dike breaching. For higher return period floods, overtopping always occurs (whatever the overtopping level and bed friction parameters) and the water level at the point of interest is directly influenced by the breach discharge (which depends on the *breach width*) and the local floodplain roughness (*FR-65537*). Moreover, the control point is located between two potential dike failure locations (*Saint-Père* and *Prouteaux* breaches). However, the dike failure at *Saint-Père*, which is located upstream from the control point, appears as the most influential factor. The *Fusible du déversoir* breach acts as a fuse plug dike clipping the flood between the 100 and 200-year return period floods. Then, other breaches (*Les Ormes* and *Prouteaux*) form along the Loire river, which increases the water depth at the control point. This finding leads to the conclusion that in a hydraulic study of inundations induced by multiple breaches, the breach development chronology affects probabilities of formation of downstream breaches, and thus the flood hazard [31], especially for flooding events close to the design conditions for river dykes. It can be noticed that water level at the control point is also controlled by friction coefficients in its neighboring zone. As expected, the riverbed and floodplain friction coefficients (identified as "PK403-414" and "FR-65537") have also an impact on the water level at low and high flow, respectively.

 doi:10.20944/preprints202210.0474.v1

5. Discussion

In this study, the effect of the uncertainty resulting from the stochastic processes of dike breaches and roughness coefficients on water level calculation for extreme flood events was investigated. The analysis presented in this work can be carried out on other quantity of interest, such as scalar flow velocity ($|\mathbf{v}|$), flood hazard index [33], total force and/or total depth indicators [14]. Based on the Froude number, the last indicator has been investigated. Since the Froude number has a limited impact in the computational domain, no significative difference is observed with the water depth analysis presented in previous section. As for quantity of interest, the methodology described in this paper can be applied for other uncertain parameters. In steady state condition, integrating breach development times has no major impact on the numerical results in comparison to instantaneous and complete breaches computation. However, in case of unsteady flow, this parameter variability in interaction to other ones (e.g. breach width) can significantly impact the dike failure probability [31]. In that case, it also could be interesting to test the influence of parametric laws for the breach expansion [41].

A major issue arising from the methodology presented in the current study concerns the optimization of the number of computational runs needed for sufficient results in the uncertainty analysis. The Monte Carlo technique, while generic and robust, is also computationally expensive due to its low convergence rate. Ways to reduce the computational cost typically require the replacement of the pure random sampling that forms the backbone of the Monte Carlo method by alternative sampling methods such as the optimized Latin Hypercube Sampling (LHS) approaches [66].

To handle the high-dimensional uncertain input space problem, special attention was paid to proposing a relevant sensitivity analysis to produce accurate and robust results. Thus, two moment independence and model free GSA methods have been investigated. Although the ranking is similar between the two methods tested, the permutation importance based on random forest provides a better distinction between influential and non-influential parameters. However, this statement needs to be completed by investigating the effect of the computation number on the sensitivity analysis methods. This was not studied here and will be the topic of a future study.

Despite the permutation importance method have informal and strong connections with Sobol' sensitivity theory [67], the method is considered in the paper as a moment independence and model free GSA method. Indeed, the permutation importance method based on Random Forest algorithm is assumed as model free since it does not make any assumptions on the model functional relationship to its inputs. In addition, no explicit statistical moment of the output variable is decomposed by the machine learning approach, that is why it is designed as moment independence method.

6. Conclusion and perspectives

The effect of uncertainty resulting from the stochastic processes of multiple dike breaches and roughness coefficients on water level calculation was investigated numerically for different extreme flood scenarios on a reach of the Loire river. It is important to recall that the results of the uncertainty analysis are directly linked to the study specification and consequently to the description of the uncertain input parameters. To address the uncertainty analysis in high dimensional spaces, a 2D depth-averaged hydraulic model was run in a Monte Carlo framework. To our knowledge, a probabilistic study including about 300 physical parameters with a 2D numerical model is not yet widespread in the environmental community and is a novelty. Inundation hazard maps for different flood scenarios highlighted the impact of the breach development chronology. To overcome the non-linearity difficulty of local phenomena, such as overtopping of a dike, moment independence and model free sensitivity analysis methods were carried out to assess the factors influencing the flow depth and flood extent. To our knowledge, this is a novelty of this work. The spatial analysis of vulnerability area induced by a levee breach width

 doi:10.20944/preprints202210.0474.v1

exhibits that, with increasing flood scenarios discharge, the rise of variable influence intensity is accompanied by a more localized spatial effect. This argues for local flood analysis to allows a sound understanding of the flood hazard for these scenarios. The physical interpretation, highlighted by the Global Sensitivity Analysis (GSA), emphasizes that interactions between breach parameters and roughness coefficients play a significant role in the water level uncertainty. For higher return periods, the weight of the uncertainty related to breach parameters seems reduced. This is probably due to the flood intensity, generating strong overtopping height and breach discharges, thus accentuating the impact of roughness coefficients.

The quantification of uncertainty in roughness coefficients was done following expert knowledge, but potentially available sources of information (e.g. *in situ* and remote sensing data) could be employed for a better characterization of the roughness coefficients in flooded areas. Another improvement to the present study is the assessment of the effect of other breach uncertain parameters (e.g. overtopping duration, widening stages and associated kinetics, breaching duration, breach shape) and other causes of breaching (e.g. piping) [18-33]. Finally, uncertainty in inundation numerical models arises from boundary conditions (state-discharge and discharge frequency curves), hydraulic model parameterization (roughness coefficient, behavior of hydraulic and protection structures) and geometric description (bathymetric and topographic data). Even if difficult, these uncertainties should also be considered from both modelers and decision-makers to propose an adapted strategy for hazard mitigation. In addition, generally uncertainty quantification studies assume independent model input parameters, which can constitute a potentially important source of approximation. Even if the dependence consideration is a source of additional complexity, it should not be neglected in uncertainty analyses [31-32].

Handling uncertainty in hydraulic study is central to sustainable and successful flood risk management [68] involving public safety and economic damage. Communicating uncertainty analysis to decision makers in order to construct a consensus for flood hazard management process is a new challenge to overcome [69].

Author Contributions: Conceptualization, C.G., V.B. and F.Z.; methodology, C.G., V.B., F.Z. and K. E.-A.; software, C.G., V.B., F.Z., K. E.-A. and S.P.; validation, C.G., V.B. and S.B.; formal analysis, C.G. and V.B.; investigation, C.G., V.B. and F.Z.; resources, C.G., V.B., F.Z., S.B and S.P.; data curation, C.G. and V.B.; writing—original draft preparation, C.G. and V.B.; writing—review and editing, F.Z., S.B., S.P. and K. E.-A.; visualization, C.G, V.B. and S.B.; supervision, C.G.; project administration, V.B. All authors have read and agreed to the published version of the manuscript.

Funding: This research received no external funding.

Data Availability Statement: Not applicable.

Acknowledgments: The authors gratefully acknowledge contributions from the open-source community, especially that of SALib (Sensitivity Analysis Library in Python) and scikit-learn (a module for Machine Learning in Python). The authors also would like to address special thanks to contributors of the very instructive and helpful website https://machinelearningmastery.com.

Conflicts of Interest: The authors declare no conflict of interest.

References

1. European Environment Agency. Economic losses and fatalities from weather- and climate-related events in Europe, 2022.
2. Freer, J.; Beven, K.J.; Neal, J.; Schumann, G.; Hall, J.; Bates, P. Flood Risk and Uncertainty. In *Risk and Uncertainty Assessment for Natural Hazards*, Cambridge, UK, 2011; pp. 190–233.
3. Ghazali, D.A.; Guericolas, M.; Thys, F.; Sarasin, F.; Arcos González, P.; Casalino, E. Climate Change Impacts on Disaster and Emergency Medicine Focusing on Mitigation Disruptive Effects: an International Perspective. *Int. J. Environ. Res. Public Health* **2018**, *15*, 1379. https://doi.org/10.3390/ijerph15071379
4. Tabari, H. Climate change impact on flood and extreme precipitation increases with water availability. *Sci Rep* **2020**, 10, 13768. https://doi.org/10.1038/s41598-020-70816-2
5. Merz, B.; Aerts, J.; Arnbjerg-Nielsen, K.; Baldi, M.; Becker, A.; Bichet, A.; Blöschl, G.; Bouwer, L.M.; Brauer, A.; Cioffi, F.; Delgado, J.M.; Gocht, M.; Guzzetti, F.; Harrigan, S.; Hirschboeck, K.; Kilsby, C.; Kron, W.; Kwon, H.-H.; Lall, U.; Merz, R.; Nissen, K.; Salvatti, P.; Swierczynski, T.; Ulbrich, U.; Viglione, A.; Ward, P.J.; Weiler, M.; Wilhelm, B.; Nied, M. Floods and climate: emerging perspectives for flood risk assessment and management. *Nat. Hazards Earth Syst. Sci.* **2014**, 14, pp. 1921–1942. https://doi.org/10.5194/nhess-14-1921-2014
6. Surminski, S.; Thieken, A.H. Promoting flood risk reduction: The role of insurance in Germany and England. *Earth's Future* **2017**, 5, pp. 979-1001. https://doi.org/10.1002/2017EF000587
7. FLOODsite. Available online: www.floodsite.net (accessed on 2009)
8. FloodProBE. Available online: www.floodprobe.eu (accessed on 2011)
9. McClymont, K.; Morrison, D.; Beevers, L.; Carmen, E. Flood resilience: a systematic review. *J. Environ. Plan. Manag.* **2020**, 63, pp. 1151-1176. https://doi.org/10.1080/09640568.2019.1641474
10. Rifai, I., Erpicum, S., Archambeau, P., Violeau, D., Pirotton, M., El kadi Abderrezzak, K., Dewals, B. Overtopping induced failure of non-cohesive homogenous dikes. *Water Resour. Res.* **2017**, 53(4), pp. 3373– 3386, https://doi.org/10.1002/2016WR020053
11. Özer, I.E.; van Damme, M.; Jonkman, S.N. Towards an International Levee Performance Database (ILPD) and Its Use for Macro-Scale Analysis of Levee Breaches and Failures. *Water*. **2020**, *12*, 119. https://doi.org/10.3390/w12010119
12. Akhter, F.; Mazzoleni, M.; Brandimarte, L. Analysis of 220 Years of Floodplain Population Dynamics in the US at Different Spatial Scales. *Water* **2021**, 13, 141. https://doi.org/10.3390/w13020141
13. FEMA (Federal Emergency Management Agency). Guidance for flood risk analysis and mapping, flood risk assessments. 2020.
14. Ferrari, A.; Dazzi, S.; Vacondio, R.; and Mignosa, P. Enhancing the resilience to flooding induced by levee breaches in lowland areas: a methodology based on numerical modelling. *Nat. Hazards Earth Syst. Sci.* **2020**, 20, pp. 59–72. https://doi.org/10.5194/nhess-20-59-2020
15. Pappenberger, F.; Beven, K.J.; Horritt, M.; Blazkova. Uncertainty in the calibration of effective roughness parameters in HEC-RAS using inundation and downstream level observations. *J. Hydrol.* **2005**, 302(1-4), pp. 46-69. https://doi.org/10.1016/j.jhydrol.2004.06.036
16. Aronica, G.T.; Franza, F.; Bates, P.D.; Neal, J.C. Probabilistic evaluation of flood hazard in urban areas using monte carlo simulation. *Hydrol. Process.* **2012**, 26(26), pp. 3962-3972. https://doi.org/10.1002/hyp.8370
17. Abily, M.; Delestre, O.; Bertrand, N.; Duluc, C.-M.; Gourbesville, P. High-resolution Modelling With Bi-dimensional Shallow Water Equations Based Codes – High-Resolution Topographic Data Use for Flood Hazard Assessment Over Urban and Industrial Environments. *Procedia Eng.* **2016**, 154, pp. 853-860. https://doi.org/10.1016/j.proeng.2016.07.453
18. Vorogushyn, S.; Merz, B.; Lindenschmidt, K.-E.; Apel, H. A new methodology for flood hazard assessment considering dike breaches. *Water Resour. Res.* **2010**, 46, W08541. https://doi.org/10.1029/2009WR008475
19. Mazzoleni, M.; Bacchi, B.; Barontini, S.; Di Baldassarre, G.; Pilotti, M.; Ranzi, R. Flooding hazard mapping in floodplain areas affected by piping breaches in the Po River, Italy. *J. Hydrol. Eng.* **2014**, 19(4), pp. 717–731. https://doi.org/10.1061/(ASCE)HE.1943-5584.0000840
20. Mazzoleni, M.; Dottori, F.; Brandimarte, L.; Tekle, S.; Martina, M.L.V. Effects of levee cover strength on flood mapping in the case of levee breach due to overtopping, *Hydrol. Sci. J.* **2017**, 62(6), pp.892-910, https://doi.org/10.1080/02626667.2016.1246800
21. Ciullo, A.; de Bruijn, K.M.; Kwakkel, J.H.; Klijn, F. Accounting for the uncertain effects of hydraulic interactions in optimising embankments heights: Proof of principle for the IJssel River. *J. Flood Risk Manag.* **2019**, 12(S2), e12532. https://doi.org/10.1111/jfr3.12532
22. Curran, A.; De Bruijn, K.M.; Kok, M. Influence of water level duration on dike breach triggering, focusing on system behaviour hazard analyses in lowland rivers. *Georisk: Assessment and Management of Risk for Engineered Systems and Geohazards* **2020**, 14(1), 26-40. https://doi.org/10.1080/17499518.2018.1542498
23. Legleiter, C.J.; Kyriakidis, P.C.; McDonald, R.R.; Nelson, J.M. Effects of uncertain topographic input data ontwo-dimensional flow modeling in a gravel-bed river. *Water Resour. Res.* **2011**, 47, W03518. https://doi.org/10.1029/2010WR009618
24. Domeneghetti, A.; Castellarin, A.; Brath, A. Assessing rating-curve uncertainty and its effects on hydraulic model calibration, *Hydrol. Earth Syst. Sci.* **2012**, 16, pp. 1191–1202. https://doi.org/10.5194/hess-16-1191-2012
25. Morvan, H.; Knight, D.; Wright, N.; Tang, X.; Crossley, A. The concept of roughness in fluvial hydraulics and its formulation in 1D, 2D and 3D numerical simulation models. *J. Hydraul. Res.* **2008**, 46(2), pp.191-208. https://doi.org/10.1080/00221686.2008.9521855
26. ASCE/EWRI Task Committee on Dam/Levee Breaching. Earthen Embankment Breaching. *J. Hydrau. Eng.* **2011**, pp. 1549–1564.

27. Dazzi, S.; Vacondio, R.; Mignosa, P. Integration of a levee breach erosion model in a GPU-accelerated 2D shallow water equations code. *Water Resour. Res.* **2019**, 55, pp. 682–702. https://doi.org/10.1029/2018WR023826
28. Tadesse, Y.B.; Fröhle, P. Modelling of Flood Inundation due to Levee Breaches: Sensitivity of Flood Inundation against Breach Process Parameters. *Water* **2020**, 12, 3566. https://doi.org/10.3390/w12123566
29. Wahl, T.L. Uncertainty of predictions of embankment dam breach parameters. *J. Hydraul. Eng.* **2004**, 130(5), pp. 389–397. https://doi.org/10.1061/(ASCE)0733-9429(2004)130:5(389)
30. Apel, H.; Merz, B.; Thieken, A.H. Influence of dike breaches on flood frequency estimation. *Comput. Geosci.* **2009**, 35(5), pp. 907-923. https://doi.org/10.1016/j.cageo.2007.11.003
31. Vorogushyn, S.; Apel, H.; Merz, B. The impact of the uncertainty of dike breach development time on flood hazard. *Phys. Chem. Earth, Parts A/B/C* **2011**, 36, pp. 319-323. https://doi.org/10.1016/j.pce.2011.01.005
32. Pheulpin, L.; Bertrand, N.; Bacchi, V. Uncertainty quantification and global sensitivity analysis with dependent inputs parameters: Application to a basic 2D-hydraulic model. *LHB* **2022**, 108:1, https://doi.org/10.1080/27678490.2021.2015265
33. D'Oria, M.; Maranzoni, A.; Mazzoleni, M. Probabilistic assessment of flood hazard due to levee breaches using fragility functions. *Water Resour. Res.* **2019**, 55, pp. 8740– 8764. https://doi.org/10.1029/2019WR025369
34. Morales-Hernandez, M., Petaccia, G., Brufau, P., and Garcıa-Navarro, P. Conservative 1D–2D coupled numerical strategies applied to river flooding: The Tiber (Rome). *Appl. Math. Model.* **2016**, 40(3), pp. 2087–2105. https://doi.org/10.1016/j.apm.2015.08.016
35. Teng, J.; Jakeman, A.J.; Vaze, J.; Croke, B.F.W.; Dutta, D.; Kim, S. Flood inundation modelling: A review of methods, recent advances and uncertainty analysis. *Environ. Model. Soft.* **2017**, 90, pp. 201-216. https://doi.org/10.1016/j.envsoft.2017.01.006
36. García-Navarro, P.; Murillo, J.; Fernández-Pato, J.; Echeverribar, I.; Morales-Hernández, M. The shallow water equations and their application to realistic cases. *Environ. Fluid. Mech.* **2019,** 19, pp. 1235–1252. https://doi.org/10.1007/s10652-018-09657-7
37. Pheulpin, L.; Bacchi, V; Bertrand, N. Comparison Between Two Hydraulic Models (1D and 2D) of the Garonne River: Application to Uncertainty Propagations and Sensitivity Analyses of Levee Breach Parameters. In *Advances in Hydroinformatics*, Gourbesville, P., Caignaert, G., Eds.; Springer, Singapore, 2020. https://doi.org/10.1007/978-981-15-5436-0_75
38. Maranzoni, A.; D'Oria, M.; Mazzoleni, M. Probabilistic flood hazard mapping considering multiple levee breaches. *Water Resour. Res.* **2022**, 58, e2021WR030874. https://doi.org/10.1029/2021WR030874
39. Huthoff, F.; Remo, J.; Pinter, N. Hydrodynamic levee-breach and inundation modelling. *J. Flood Risk Manage.* **2015**, 8, pp. 2-18. https://doi.org/10.1111/jfr3.12066
40. Hervouet, J.-M. *Hydrodynamics of Free Surface Flows: Modelling With the Finite Element Method*; Publisher: John Wiley & Sons, Chichester, England, 2007.
41. Kheloui, L.; El Kadi Abderrezzak, K.; Bourban, S. Simplified physically-based modelling of overtopping induced levee breaching with TELEMAC-2D. In Proceedings of the *TELEMAC-MASCARET User Conference*, Antwerp, Belgium, October 2021.
42. Hervouet, J.-M.; Bates, P. The TELEMAC modelling system Special issue. *Hydrol. Process.* **2000**, 14, 2207-2208. https://doi.org/10.1002/1099-1085(200009)14:13<2207::AID-HYP22>3.0.CO;2-B
43. Morvan, H.; Knight, D.; Wright, N.; Tang, X.; Crossley, A. The concept of roughness in fluvial hydraulics and its formulation in 1D, 2D and 3D numerical simulation models. *J. Hydraul. Res.* **2008**, 46(2), pp. 191-208. https://doi.org/10.1080/00221686.2008.9521855
44. HydroPortail. Available online: http://www.hydro.eaufrance.fr (accessed on 2016)
45. Copernicus Land Monitoring Service. Available online: https://land.copernicus.eu/pan-european/corine-land-cover (accessed on 2011)
46. Maurin, J.; Boulay, A.; Piney, S.; Le Barbu, E.; Tourment, R. Les brèches des levées de la Loire : brèche de Jargeau 1856. In Proceedings of the *Congrès SHF Événements extrêmes fluviaux et maritimes*, Paris, France, 2012.
47. DREAL. Études de dangers des digues de classe A de la Loire moyenne Éléments de synthèse relatifs à l'analyse des brèches historiques, 2012.
48. Rifai, I.; El Kadi Abderrezzak, K.; Erpicum, S.; Archambeau, P.; Violeau, D.; Pirotton, M.; Dewals, B. Floodplain backwater effect on overtopping induced fluvial dike failure. *Water Resour. Res.* **2018**, 54, pp. 9060– 9073. https://doi.org/10.1029/2017WR022492
49. Wu, W.; Li, H. A simplified physically-based model for coastal dike and barrier breaching by overtopping flow and waves. *Coast. Eng.* **2017**, 130, pp.1-13. https://doi.org/10.1016/j.coastaleng.2017.09.007
50. Goeury, C.; Audouin, Y.; Zaoui, F. Interoperability and computational framework for simulating open channel hydraulics: Application to sensitivity analysis and calibration of Gironde estuary model. *Environ. Model. Softw.* **2022**, 148. https://doi.org/10.1016/j.envsoft.2021.105243
51. Auriau, L.; Mériaux, P.; Royet, P.; Tourment, R.; Lacombe, S.; Maurin, J.; Boulay, A. FloodProBE Project WP 3: Reliability of Urban Flood Defences. Guidebook for Using Helicopter-Borne Lidar to Contribute to Levee Assessment – Experiment on "Val d'Orléans" Pilot Site, IRSTEA, 2012. https://hal.inrae.fr/hal-02600693
52. Zomorodi, K. Empirical Equations for Levee Breach Parameters Based on Reliable International Data. In Proceedings of the Dam Safety 2020, Association of State Dam Safety Officials, Virtual Conference, September 2020.
53. Resio, D.T.; Boc, S.J.; Maynord, S.; Ward, D.; Abraham, D.; Dudeck, D.; Welsh. B. Development and Demonstration of Rapid Repair of Levee Breaching Technology, Report to Department of Homeland Security, 2009.
54. U.S. Bureau of Reclamation (USBR). Downstream Hazard Classification Guidelines, ACER Technical Memorandum No. 11. U.S. Bureau of Reclamation, U.S. Department of the Interior, Denver, 1988.

55. Sobol', I.M. Global sensitivity indices for nonlinear mathematical models and their monte carlo estimates. *Math. Comput. Simul.* **2001**, 55(1-3), pp. 271-280. https://doi.org/10.1016/S0378-4754(00)00270-6
56. Saltelli, A. Making best use of model evaluations to compute sensitivity indices. *Comput. Phys. Comm.* **2002**, 145(2), pp. 280-297. https://doi.org/10.1016/S0010-4655(02)00280-1
57. Sudret, B. Global sensitivity analysis using polynomial chaos expansions. *Reliab. Eng. Syst. Saf.* **2008**, 93(7), pp. 964-979. https://doi.org/10.1016/j.ress.2007.04.002
58. Pappenberger, F.; Beven, K.J.; Ratto, M.; Matgen, P. Multi-method global sensitivity analysis of flood inundation models. Adv. *Water Resour.* **2008**, 31(1), pp. 1-14. https://doi.org/10.1016/j.advwatres.2007.04.009
59. Saltelli, A. Sensitivity analysis for importance assessment. *Risk Anal.* **2002**, 22(3), pp. 579-590. https://doi.org/10.1111/0272-4332.00040
60. Borgonovo, E. A new uncertainty importance measure. *Reliab. Eng. Syst. Saf.* **2007**, 92(6), pp. 771-784. https://doi.org/10.1016/j.ress.2006.04.015
61. Breiman, L. Random Forests. *Mach. Learn.* **2021**, 45, pp. 5-32. https://doi.org/10.1023/A:1010950718922
62. Pedregosa, F.; Varoquaux, G.; Gramfort, A.; Michel, V.; Thirion, B.; Grisel, O.; Blondel, M.; Prettenhofer, P.; Weiss, R.; Dubourg, V.; Vanderplas, J.; Passos, A.; Cournapeau, D.; Brucher, M.; Perrot, M.; Duchesnay, E. Scikit-learn: Machine Learning in Python. *J. Mach. Learn. Res.* **2011**. 12, pp. 2825-2830.
63. Plischke, E.; Borgonovo, E.; Smith, C.L. Global sensitivity measures from given data. *European J. Oper. Res.* **2013**, 226 (3), pp. 536-550. https://doi.org/10.1016/j.ejor.2012.11.047
64. Herman, J.; Usher, W. SALib: An open-source Python library for Sensitivity Analysis. *J. Open Source Softw.* **2017**. 2(9), 97. https://doi.org/10.21105/joss.00097
65. Brody, S.D.; Kang, J.E.; Bernhardt, S. Identifying factors influencing flood mitigation at the local level in Texas and Florida: the role of organizational capacity. *Nat. Hazards* **2010**. 52, pp. 167–184. https://doi.org/10.1007/s11069-009-9364-5
66. Damblin, G.; Couplet, M.; Iooss, B. Numerical studies of space-filling designs: optimization of Latin Hypercube Samples and subprojection properties. *J. Simul.* **2013,** 7(4), pp. 276-289. https://doi.org/10.1057/jos.2013.16
67. Razavi, S.; Jakeman, A.; Saltelli, A.; Prieur, C.; Iooss, B.; Borgonovo, E.; Plischke, E.; Lo Piano, S.; Iwanaga, T.; Becker, W.; Tarantola, S.; Guillaume, J.H.A.; Jakeman, J.; Gupta, H.; Melillo, N.; Rabitti, G.; Chabridon, V.; Duan, Q.; Sun, X.; Smith, S.; Sheikholeslami, R.; Hosseini, N.; Asadzadeh, M.; Puy, A.; Kucherenko, S.; Maier, H. R. The future of sensitivity analysis: an essential discipline for systems modeling and policy support. *Environ. Model. Softw.* **2021**, 137. https://doi.org/10.1016/j.ejor.2021.11.018
68. Jonkman, S.N.; Dawson, R.J. Issues and Challenges in Flood Risk Management—Editorial for the Special Issue on Flood Risk Management. *Water* **2012**. 4, pp. 785-792. https://doi.org/10.3390/w4040785
69. Hall, J.; Solomatine, D. A framework for uncertainty analysis in flood risk management decisions. *Int. J. River Basin Manag.* **2008**, 6(2), pp. 85-98. https://doi.org/10.1080/15715124.2008.9635339